EFFECT OF STRESS RATIO ON FATIGUE-CRACK GROWTH IN 7075-T6 ALUMINUM-ALLOY SHEET

By C. Michael Hudson and Joseph T. Scardina

NASA Langley Research Center
Langley Station, Hampton, Va.

Presented at the National Symposium on Fracture Mechanics
- Bethlehem, Pennsylvania
June 19-21, 1967

EFFECT OF STRESS RATIO ON FATIGUE-CRACK GROWTH IN 7075-T6 ALUMINUM-ALLOY SHEET

By C. Michael Hudson and Joseph T. Scardina

ABSTRACT

Axial-load fatigue-crack-propagation tests were conducted on 12-inch-(305-mm) wide sheet specimens made of 7075-T6 aluminum alloy. These tests were made at stress ratios R (ratio of the minimum stress to the maximum stress) ranging from -1.0 to 0.8 and at maximum stress levels ranging from 5 to 50 ksi (34 to 340 MN/m^2) to study the effects of stress ratio on fatigue-crack growth. The fatigue-crack-propagation data were analyzed using Paris' stress-intensity analysis. The data from tests at negative R values fell into a relatively narrow scatterband along with the results from the R = 0 tests on a plot of rate against stress-intensity range. Apparently, the compression portion of the loading cycle did not significantly affect crack growth in these tests. The data from tests at different positive stress ratios fell into discrete bands on these plots. These bands varied systematically with R, that is, the higher the stress ratio at a given value of ΔK, the higher the rate of fatigue-crack growth. This spread in rates was small at the lower stress-intensity range, but became progressively larger as the stress-intensity range was increased.

Semiempirical equations developed by Forman, et al., by Broek and Schijve, and by Paris were fitted to the data from this investigation using a least squares fit. Forman's equation gave the best fit to the data.

The fracture surfaces of the specimens changed from the normal mode to a shear mode within a reasonably narrow range of crack growth rates for all R values. The stress-intensity range at transition was approximately a constant for tests at negative stress ratios. Forman's equation adequately represented the variation between the stress ratio and the stress-intensity range at positive stress ratios.

EFFECT OF STRESS RATIO ON FATIGUE-CRACK GROWTH IN 7075-T6 ALUMINUM-ALLOY SHEET

By C. Michael Hudson* and Joseph T. Scardina**

NASA Langley Research Center
Langley Station, Hampton, Va.

INTRODUCTION

Fatigue cracks frequently grow during a large portion of the life of cyclically loaded components. Therefore, any parameter which significantly affects the growth of fatigue cracks can have a major effect on the total fatigue behavior of the components. One such parameter is the stress ratio R (ratio of the minimum stress to the maximum stress). Accordingly, an investigation has been conducted to determine the effects of a wide range of R values and stresses on fatigue-crack growth in 7075-T6 aluminum-alloy sheet specimens. This material was selected because of its frequent use in aircraft construction.

The data were analyzed using Paris' stress-intensity method (ref. 1) which is based on fracture mechanics considerations. Figge and Newman (ref. 2) showed that by using this method the data from simple sheet specimens could be used to predict fatigue-crack-growth behavior in simulated structural configurations. Semiempirical equations developed by Forman, et al. (ref. 3), by Broek and Schijve (ref. 4), and by Paris (ref. 1) were fitted to the data generated in this investigation using least squares techniques.

The crack lengths and crack propagation rates at the transition from the normal to the shear mode on the failure surfaces were determined. A study was made to determine whether a relationship existed between the stress ratio and the stress-intensity range at transition.

SYMBOLS

The units used for the physical quantities defined in this paper are given both in U.S. Customary Units and in the International System of Units, SI (ref. 5). The appendix presents factors relating these two systems of units.

a one-half of the total length of a central symmetrical crack, in. (mm)

a_f half-length of crack immediately prior to rapid fracture, in. (mm)

---

*Materials Engineer.
**Aerospace Engineer.

a_i half-length of crack at onset of slow crack growth, in. (mm)

a_t half-length of crack at which transition of the failure surface from the normal mode to the shear mode began, in. (mm)

C, C_1, C_2, C_3 constants in fatigue-crack propagation equations

K_c critical stress-intensity factor for failure, psi-$in^{1/2}$ $\left(MN/m^{3/2}\right)$

K_{max} stress-intensity factor corresponding to maximum cyclic stress, using tangent formula width correction, psi-$in^{1/2}$ $\left(MN/m^{3/2}\right)$

K'_{max} stress-intensity factor corresponding to maximum cyclic stress, using Broek's width correction, psi-$in^{1/2}$ $\left(MN/m^{3/2}\right)$

K_{min} stress-intensity factor corresponding to minimum cyclic stress, using tangent formula width correction, psi-$in^{1/2}$ $\left(MN/m^{3/2}\right)$

K'_{min} stress-intensity factor corresponding to minimum cyclic stress by using Broek's width correction, psi-$in^{1/2}$ $\left(MN/m^{3/2}\right)$

ΔK range of the stress-intensity factor (with tangent width correction), $K_{max} - K_{min}$, psi-$in^{1/2}$ $\left(MN/m^{3/2}\right)$

ΔK_t range of the stress-intensity factor at transition, psi-$in^{1/2}$ $\left(MN/m^{3/2}\right)$

$\Delta K'$ range of the stress-intensity factor (with Broek's width correction), psi-$in^{1/2}$ $\left(MN/m^{3/2}\right)$

m, n exponents in fatigue-crack-growth equation

N number of cycles

P_a alternating load, kips (newtons)

P_f load on specimen immediately prior to rapid fracture, kips (newtons)

P_i load on specimen at onset of slow crack growth, kips (newtons)

P_m mean load, kips (newtons)

P_{max} maximum load applied in a cycle, $P_m + P_a$, kips (newtons)

P_{min}	minimum load applied in a cycle, $P_m - P_a$, kips (newtons)
R	ratio of minimum stress to maximum stress
S'_a	alternating net stress, $P_a/(w - x)t$, ksi (MN/m^2)
S'_m	mean net stress, $P_m/(w - x)t$, ksi (MN/m^2)
S_{max}	maximum gross stress, P_{max}/wt, ksi (MN/m^2)
S_{min}	minimum gross stress, P_{min}/wt, ksi (MN/m^2)
S_o	maximum net stress, $P_{max}/(w - x)t$, ksi (MN/m^2)
t	specimen thickness, in. (mm)
w	specimen width, in. (mm)
x	length of the crack starter notch, in. (mm)
α	correction for finite width of panel

SPECIMENS, TESTS, AND PROCEDURES

Specimens

The material was taken from the special stock of 7075-T6 aluminum-alloy sheet retained at Langley Research Center for fatigue testing. The fatigue properties of this material are discussed in reference 6. The tensile properties of the sheet are given in table I. The specimen configuration is shown in figure 1. Sheet specimens 12 inches wide (305 mm), 35 inches (891 mm) long, and with a nominal thickness of 0.090 inch (2.28 mm) were tested.

A notch 0.10 inch (2.5 mm) long by 0.01 inch (0.25 mm) wide was cut into the center of each specimen using an electrical discharge process. Very localized heating occurs in making notches in this manner. Thus, virtually all of the material through which the fatigue crack propagates is unaltered by the cutting process. All specimens were made with the longitudinal axis of the specimens parallel to the rolling direction of the sheet.

A reference grid (ref. 7) was photographically printed on the surface of the specimens to mark intervals in the path of the crack. Metallographic examination and tensile tests conducted on specimens bearing the grid indicated that the grid had no detrimental effect on the material.

Testing Machines

Four axial-load fatigue testing machines were employed in this investigation: a 20,000-lbf- (89-kN) capacity subresonant fatigue machine (ref. 8) having an operating frequency of 1800 cpm (30 Hz); a 100,000-lbf- (445-kN) capacity hydraulic fatigue machine (ref. 9) which applied loads at a rate of 1200 cpm (20 Hz); a 120,000-lbf- (553-kN) capacity jack (ref. 10) having a loading frequency of 30 cpm (0.5 Hz), and a combination hydraulic and subresonant fatigue testing machine (ref. 11) capable of applying loads up to 132,000 pounds (587 kN) hydraulically or 105,000 pounds (466 kN) subresonantly. The operating frequencies were 40 to 60 cpm (0.7 to 1 Hz) for the hydraulic unit, and approximately 820 cpm (14 Hz) for the subresonant unit.

Loads were continuously monitored on these machines by measuring the output of a strain-gage bridge attached to a dynamometer in series with the specimens. The maximum error in loading was ±1 percent of the applied load.

Test Procedure

Axial-load fatigue-crack-propagation tests were conducted at stress ratios ranging from -1.0 to 0.8. Generally, tests were conducted at a number of stress levels (ranging from 5 to 50 ksi (34 to 340 MN/m^2)) for a given stress ratio. Duplicate tests were conducted at each stress level. The mean and alternating loads were kept constant throughout each test.

Fatigue crack growth was observed through 10-power microscopes while illuminating the specimen with stroboscopic light. The number of cycles required to propagate the crack to each grid line was recorded so that crack-propagation rates could be determined. Approximately two-thirds of the crack-propagation tests were conducted to failure. The remaining one-third were stopped before failure, and the cracked specimens used in residual-static-strength tests.

In all of the tests (crack growth and residual static strength), the specimens were clamped between lubricated guides in order to prevent buckling and out-of-plane vibrations during testing. Light oil was used to lubricate the surfaces of the specimens and the guides. None of this oil was observed to enter the crack during testing. Consequently, the oil was not expected to affect the crack growth. Ethyl alcohol was periodically sprayed on the specimen surface to more clearly indicate the crack front. A cutout 1/8 inch (3.18 mm) wide was made across the width of one guide plate to allow visual observation of the crack-growth region.

Axial-load residual-static-strength tests were conducted at a load rate of 120,000 lbf/min (10 kN/s), using the unfailed crack-propagation specimens. A 70-mm sequence camera operating at 20 frames per second was used to obtain slow crack-growth data. The cracked section of the specimen and the image of a load-indicating device were photographed on each frame of film by using an optical prism. From this film, the load at which the crack first started to grow statically and the load and crack length immediately prior to final failure were determined.

Method of Analysis

The fatigue-crack-growth data were analyzed by using the stress-intensity method (ref. 1) which is based on fracture mechanics considerations. This method hypothesized that the rate of fatigue-crack propagation was a function of the stress-intensity range, that is

$$\frac{da}{dN} = f(\Delta K) \tag{1}$$

where

$$\Delta K = K_{max} - K_{min} \tag{2}$$

For centrally cracked specimens subjected to a uniformly distributed axial load

$$K_{max} = S_{max}\sqrt{a}\alpha \tag{3}$$

and

$$K_{min} = S_{min}\sqrt{a}\alpha \tag{4}$$

The term α is a factor which corrects for the finite width of the specimen and is given by:

$$\alpha = \sqrt{\frac{w}{\pi a} \tan \frac{\pi a}{w}} \tag{5}$$

The term S_{max} is the maximum gross stress in the cycle and S_{min} is the minimum gross stress in the cycle. In presenting the results, the experimental values of da/dN were plotted against ΔK (eq. (2)).

RESULTS AND DISCUSSION

Fatigue-Crack-Growth Rates

The fatigue-crack-growth curves (plots of half-crack length against number of cycles) from duplicate tests were plotted on a single figure, and an average curve derived. The difference in the number of cycles required to reach a given crack length in duplicate tests seldom exceeded 20 percent. All of the fatigue-crack-growth data presented in the next three sections were obtained from these average curves. The number of cycles required to propagate the cracks from a half-length a of 0.10 in. (2.54 mm) to specified half-crack lengths is shown in table II. Fatigue-crack-propagation rates, da/dN, were determined graphically by taking the slopes of the crack-growth curves defined in table II.

Effect of Stress Ratio

The fatigue-crack-propagation data are presented in plots of rate against the stress-intensity range ΔK. The data from tests at all negative R values fell into a relatively narrow scatterband along with the data from $R = 0$ tests (see fig. 2) when the compression portion of the loading cycle was neglected in calculating ΔK. That is, for $R < 0$, ΔK in equation (2) became K_{max}. Apparently, the compression portion of the loading cycle did not significantly affect fatigue-crack growth in these tests. This finding is consistent with that of Illg and McEvily (ref. 12) who found no effect of compressive loading on crack propagation in a limited number of tests on 7075-T6.

The data from all tests at a given positive R value fell into a discrete scatterband on the plots of rate against ΔK (fig. 3). These scatterbands varied systematically with R, that is, the higher the stress ratio, the higher the rate of fatigue-crack growth for a given value of ΔK. This spread in rates for different values of R became larger as ΔK increased. In contrast to this finding, all of the data from tests at R values ranging from 0 to 0.85 fell into the same scatterband for Ti-8Al-1Mo-1V (Duplex Annealed), ref. 13.

Correlation of Data With Fatigue-Crack Growth

Empirical fatigue-crack-growth equations developed by Forman, et al., (ref. 3), by Broek and Schijve (ref. 4), and by Paris (ref. 1) were fitted to the test data. Forman's and Broek's equations contained R as an explicit function while Paris' equation did not. Least squares techniques were used to determine the appropriate constants for the various equations. (NOTE: The constants given in this report for these equations are for U.S. Customary Units only!) In fitting these equations, all of the data from $R < 0$ tests were assumed to apply to $R = 0$ tests since all of the data for $R \leq 0$ fell into the same scatterband.

The empirical equation developed by Forman, et al. (ref. 3), relating da/dN, ΔK, R, and K_c (the critical stress-intensity factor at failure) produced excellent fit to the data (fig. 4). This equation has the form:

$$\frac{da}{dN} = \frac{C(\Delta K)^n}{(1 - R)K_c - \Delta K} \tag{6}$$

where C and n are empirically determined constants. The value of K_c was obtained from the auxiliary residual static strength tests. This factor is related to the load at rapid fracture P_f, the associated crack length a_f, and the width-correction factor α as follows:

$$K_c = \left(P_f/wt\right)\sqrt{a_f}\alpha \tag{7}$$

An average value of K_c of 40,400 psi-in$^{1/2}$ (40.7 MN/m$^{3/2}$) was found in these tests (table III). The constants C and n in equation (6) were calculated to have values of 2.13×10^{-13} and 3.21, respectively. These values are close to the values obtained in reference 3 for 7075-T6 aluminum-alloy sheet tested at a limited number of stress ratios.

The equation developed by Broek and Schijve (ref. 4) was also fitted to the test data (fig. 5). This equation has the form:

$$\frac{da}{dN} = C_1\left(K'_{max}\right)^3 \exp\left(-C_2 R\right) \tag{8}$$

where

$$K'_{max} = S_{max}\sqrt{a}\ \sqrt[3]{1 + 40(a/w)^2} \tag{9}$$

Equation (8) can also be written in terms of the stress-intensity range as

$$\frac{da}{dN} = C_1\left(\frac{\Delta K'}{1 - R}\right)^3 \exp\left(-C_2 R\right) \tag{10}$$

The constants C_1 and C_2 were determined to be 6.93×10^{-17} and 3.85, respectively. The curves computed by equation (10) are shown in figure 5. Broek's equation does not fit the test data particularly well, especially at the higher crack-growth rates for either positive, zero, or negative R values. The sums of the squares of the differences between the logarithms of the observed rates and those of the calculated rates were three times larger for Broek's equation than for Forman's. (These are the sums which were minimized by using least squares techniques.)

Paris (ref. 1) proposed the following relationship between the rate of fatigue-crack growth and the stress-intensity range:

$$\frac{da}{dN} = C_3(\Delta K)^m \tag{11}$$

where C_3 is a constant which is proposed to incorporate the effects of material, mean load, loading frequency, and environment. (The functional form of eq. (11) is shown by eq. (1).) Paris found the broad trend of the data is characterized by equation (11) where $m = 4$. This equation produced a reasonably good fit to the data (fig. 6). Separate values of the coefficient C_3 had to be computed for each R value since R is not an explicit function in equation (11). These coefficients are listed in the following table:

R	C_3
≤ 0	5.52×10^{-21}
.2	6.44×10^{-21}
.33	1.00×10^{-20}
.5	1.80×10^{-20}
.7	3.95×10^{-20}
.8	6.84×10^{-20}

Comparison of figures 4 and 6 shows that Forman's equation fits the data from this investigation somewhat better than Paris'. The sum of the squares of the differences between the logarithms of the observed rates and those of the calculated rates was one and one-half times larger for Paris' equation than for Forman's. The superiority of Forman's equation is even further exemplified by the fact that it fit the data better with only two empirical constants than Paris' equation did with six.

The data on each plot in figure 4 fell in a narrow band that has an "S" shape or reflex type of curvature. A reflex curvature is also obtained from Forman's equation, which is induced by ΔK approaching $(1 - R)K_c$ in the denominator of equation (6). This intrinsic shape is the primary reason for the excellent fit obtained using Forman's equation. Broek's and Paris' equations do not provide for this reflex curvature.

Fatigue-Crack-Growth Behavior at Transition in Fracture Mode

The fracture surfaces of the broken specimens were inspected to determine the crack lengths at which the transition from the normal mode (fracture surface normal to the sheet surface and loading direction) to a shear mode (fracture surface 45° to the sheet surface) began. The values of da/dN, ΔK, and R associated with transition in each test are listed in table IV. (NOTE: The rates at transition listed in table IV were obtained from the crack-growth curves for the individual tests rather than from the average curves in table II.) The transitions began within a reasonably narrow range of crack-growth rates (8.8×10^{-6} to 2.9×10^{-5} in./cycle (200 to 730 nm/cycle)) for all R values. Broek and Schijve (ref. 4) similarly found that the rate of crack growth was approximately constant when the transition was completed rather than beginning.

In 45 of the 92 tests conducted, the transition to the shear mode began at the crack starter notch. The value of a_t in these tests has been designated ≤ 0.05 in. (13 mm) in table IV. The fatigue-crack-growth rates measured in these 45 tests were never lower than 2.9×10^{-5} in./cycle (730 nm/cycle),

the apparent upper limit of the range of rates at transition for the remaining tests.

The stress-intensity range at transition ΔK_t was approximately a constant for $R \leq 0$ (fig. 7). At $R > 0$, Forman's equation (eq. (6)) gave a good approximation of the relationship between ΔK and R when a crack-growth rate of 1.40×10^{-5} in./cycle (which is within the narrow range of crack-growth rates at transition) was assumed at transition (see fig. 7). The values of C, n, and K_c were known as discussed previously. Substituting these values into equation (6) gave the following nonlinear relationship between ΔK and R at transition for these tests:

$$R = 1 - \frac{1.52 \times 10^{-8}(\Delta K)^{3.21} + \Delta K}{40400} \tag{12}$$

Contrary to this finding, Wilhem (ref. 14) reported a linear relationship between ΔK and R at transition for aluminum alloys tested at positive R values.

At transition the fracture surfaces changed from the normal mode to single, double, or dual (single at one end of the crack and double at the other) shear mode (see table IV). No relationship was apparent between the type of shear mode (single, double, or dual) and the applied stress level.

CONCLUSIONS

Axial-load fatigue-crack-propagation tests were conducted on sheet specimens 12 in. (305 mm) wide and nominally 0.090 in. (2.28 mm) thick made of 7075-T6 aluminum alloy. These tests were at stress ratios R ranging from -1.0 to 0.8, and at maximum stresses ranging from 5 to 50 ksi (34 to 340 MN/m^2) to study the effect of R on fatigue-crack growth. The test results were analyzed using the stress-intensity method and correlated with three empirical relations. The following conclusions can be drawn from this study:

1. In plots of crack-growth rates against the stress-intensity range, all of the data from tests at negative R values fell into a relatively narrow scatterband with the data from the $R = 0$ tests indicating that the compression portion of the loading cycle did not significantly affect crack growth in these tests.

2. In contrast the data from all tests at a given positive R value fell into discrete bands in the plots of rate against stress-intensity range. These bands varied systematically with R, that is, the higher the stress ratio, the higher the rate of fatigue-crack growth for a given value of ΔK. The spreads in rates for different values of R became larger as ΔK increased.

3. Empirical equations developed by Forman, et al., and by Broek and Schijve which present the rate as a function of stress-intensity range, stress

ratio, and the critical stress-intensity factor for failure (Forman's equation only) were fitted to the data. Forman's equation produced an excellent fit to the data whereas Broek's equation did not correlate well at the higher crack-growth rates. Forman's equation can be used to predict fatigue-crack-growth behavior in 7075-T6 aluminum-alloy sheet for any loading condition for which the applied stress-intensity range can be calculated.

4. An empirical equation developed by Paris relating rate to the stress-intensity range produced a reasonably good fit to the data for a given value of R. However, R is not an explicit function in Paris' equation and individual constants are required for each value of R.

5. The fracture surfaces of the specimens changed from the normal mode to a shear mode within a reasonably narrow range of crack-growth rates for all R values.

6. The stress-intensity factor range at transition from the normal to the shear fracture mode was approximately a constant for tests at negative-stress ratios. Forman's equation adequately represented the variation between the stress ratio and the stress-intensity range at positive-stress ratios for transition conditions.

APPENDIX

CONVERSION OF U.S. CUSTOMARY UNITS TO SI UNITS

The International System of Units (SI) was adopted by the Eleventh General Conference of Weights and Measures, Paris, October 1960, in Resolution No. 12 (ref. 4). Conversion factors for the units used herein are given in the following table:

To convert from U.S. Customary Units	Multiply by	To obtain SI Units
lbf	4.448222	newton (N)
in.	2.54×10^{-2}	meter (M)
ksi	6.894757	newton/meter^2 (N/m^2)
cpm	1.67×10^{-2}	hertz (Hz)

Prefixes and symbols to indicate multiples of units are as follows:

Multiple	Prefix	Symbol
10^{-9}	nano	n
10^{-3}	milli	m
10^{3}	kilo	k
10^{6}	mega	M
10^{9}	giga	G

REFERENCES

1. Paris, Paul C.: The Fracture Mechanics Approach to Fatigue. Fatigue – An Interdisciplinary Approach. John J. Burke, Norman L. Reed, and Volker Weiss, Syracuse Univ. Press, 1964.

2. Figge, I. E.; and Newman, J. C., Jr.: Fatigue Crack Propagation in Structures With Simulated Rivet Forces. Paper No. 30 presented at the ASTM Annual Meeting held in Atlantic City, June 27-July 1, 1966.

3. Forman, R. G.; Kearney, V. E.; and Engle, R. M.: Numerical Analysis of Crack Propagation in Cyclically Loaded Structures. Presented at the 1966 ASME Annual Winter Meeting. Paper No. 66, WA/MET-4, Nov. 1966.

4. Broek, D.; and Schijve, J.: The Influence of the Mean Stress on the Propagation of Fatigue Cracks in Aluminum Alloy Sheet. NLR-TR M.2111, 1963.

5. Mechtly, E. A.: The International System of Units – Physical Constants and Conversion Factors. NASA SP-7012, 1964.

6. Grover, H. J.; Bishop, S. M.; and Jackson, L. R.: Fatigue Strengths of Aircraft Materials. Axial-Load Fatigue Tests on Unnotched Sheet Specimens of 24S-T3 and 75S-T6 Aluminum Alloys and of SAE 4130 Steel. NACA TN 2324, 1951.

7. Hudson, C. Michael: Fatigue-Crack Propagation in Several Titanium and Stainless-Steel Alloys and One Superalloy. NASA TN D-2331, 1964.

8. Grover, H. J.; Hyler, W. S.; Kuhn, Paul; Landers, Charles B.; and Howell, F. M.: Axial-Load Fatigue Properties of 24S-T and 75S-T Aluminum Alloy as Determined at Several Laboratories. NACA Rept. 1190, 1954 (Supersedes NACA TN 2928).

9. McEvily, Arthur J., Jr.; and Illg, Walter: The Rate of Fatigue-Crack Propagation in Two Aluminum Alloys. NACA TN 4394, 1958.

10. Illg, Walter: Fatigue Tests on Notched and Unnotched Sheet Specimens Made of 2024-T3 and 7075-T6 Aluminum Alloys and of SAE 4130 Steel With Special Consideration of the Life Range From 2 to 10,000 Cycles. NACA TN 3866, 1956.

11. Hudson, C. Michael; and Hardrath, Herbert F.: Investigation of the Effects of Variable-Amplitude Loadings on Fatigue Crack Propagation Patterns. NASA TN D-1803, 1963.

12. Illg, Walter; and McEvily, Arthur J., Jr.: The Rate of Fatigue-Crack Propagation for Two Aluminum Alloys Under Completely Reversed Loading. NASA TN D-52, 1959.

13. Hudson, C. Michael: Investigation of Fatigue Crack Growth in Ti-8Al-1Mo-1V (Duplex Annealed) Specimens Having Various Widths. NASA TN D-3879, 1967.

14. Wilhem, D. P.: Crack Propagation and Stress Intensity Interrelationships Accompanying Fatigue on Sheet Materials. SESA Paper No. 1173, Nov. 1966.

TABLE I.- AVERAGE TENSILE PROPERTIES OF

THE 7075-T6 ALUMINUM-ALLOY TESTED

Ultimate tensile strength		Yield strength (0.2-percent offset)		Young's modulus of elasticity		Elongation in 2-inch (51 mm) gage length, percent	Number of tests
ksi	MN/m^2	ksi	MN/m^2	ksi	GN/m^2		
82.9	572	75.5	521	10.2×10^3	70.3	12	152

TABLE II.- AVERAGE NUMBER OF CYCLES REQUIRED TO EXTEND CRACKS FROM A HALF-LENGTH OF 0.10 INCH (2.54 mm) IN 7075-T6 ALUMINUM-ALLOY SHEET

S_m		S_a		Nominal R value	Number of cycles required to propagate a crack from a half-length a of 0.10 in. (2.54 mm) to a half-length a of -													
ksi	MN/m^2	ksi	MN/m^2		0.20 in. (5.08 mm)	0.30 in. (7.62 mm)	0.40 in. (10.16 mm)	0.50 in. (12.70 mm)	0.60 in. (15.24 mm)	0.70 in. (17.78 mm)	0.80 in. (20.32 mm)	0.90 in. (22.86 mm)	1.00 in. (25.40 mm)	1.20 in. (30.48 mm)	1.40 in. (35.56 mm)	1.60 in. (40.64 mm)	1.80 in. (45.72 mm)	2.00 in. (50.80 mm)	2.40 in. (60.96 mm)
0	0	30	207	-1	1,240	1,640	1,865	1,980	2,040	2,080	2,110	2,120	2,140						
0	0	25	172	-1	3,230	4,200	4,600	4,860	5,000	5,100	5,160	5,200	5,270	5,330	5,370				
0	0	20	138	-1	4,820	7,170	8,450	9,180	9,600	9,900	10,060	10,200	10,250						
0	0	15	103	-1	8,000	12,500	15,300	17,300	18,830	19,900	20,700	21,300	21,830	22,700	23,300				
0	0	10	69	-1	30,000	43,800	52,000	58,100	63,400	67,300	71,000	74,000	76,800	81,100	84,000	86,000			
0	0	5	34	-1	492,000	770,000	867,000	920,000	960,000	985,000	1,007,000	1,020,000	1,040,000	1,065,000	1,083,000	1,098,000	1,110,000	1,120,000	1,138,000
2.5	17	20	138	-.8	2,500	3,730	4,380	4,760	5,000	5,150	5,280	5,370	5,440						
2.5	17	17.5	121	-.8	5,720	8,700	10,080	10,860	11,370	11,700	11,920	12,120	12,260	12,440					
5	34	25	172	-.7	1,375	1,900	2,160	2,320	2,410	2,475	2,525	2,570	2,600	2,640	2,660				
2.5	17	15	103	-.7	5,900	8,500	10,200	11,300	12,130	12,700	13,200	13,500	13,780	14,100	14,360				
2.5	17	12.5	86	-.7	11,400	16,800	20,100	22,200	23,800	24,800	25,600	26,200	26,700	27,400	27,700				
5	34	20	138	-.6	2,640	3,740	4,300	4,640	4,850	5,000	5,100	5,170	5,230	5,270					
2.5	17	10	69	-.6	16,600	24,200	28,500	31,700	34,000	35,800	37,400	38,700	39,900	41,400	42,500	43,100	43,600		
5	34	15	103	-.5	5,300	7,900	9,730	10,680	11,200	11,550	11,800	11,970	12,060	12,200					
10	69	20	138	-.33	1,550	2,100	2,350	2,470	2,540	2,580	2,600	2,630	2,633						
5	34	10	69	-.33	12,300	18,300	22,000	24,500	26,600	28,200	29,300	30,200							
2.5	17	5	34	-.33	140,000	186,000	209,000	223,000	233,000	241,000	248,000	252,000	257,000	264,000	270,000	273,000	276,000		
20	138	30	207	-.2	226	294	316	322	324										
10	69	15	103	-.2	2,900	4,300	4,930	5,300	5,540	5,700	5,800	5,900	5,990	6,100	6,160	6,180			
15	103	20	138	-.14	1,060	1,380	1,545	1,630	1,680	1,710	1,730								
25	172	25	172	0	330	413													
20	138	20	138	0	700	930	1,030	1,075	1,100	1,110									
15	103	15	103	0	1,670	2,360	2,660	2,820	2,930	3,000	3,050								
10	69	10	69	0	6,140	8,800	10,370	11,300	11,800	12,300	12,570	12,800	12,950	13,150					
5	34	5	34	0	70,000	88,300	98,300	105,000	110,000	113,000	117,000	120,000	122,000	127,000	129,000	131,000	132,000		
30	207	20	138	.2	410	490													
25	172	16.7	115	.2	760	990	1,100	1,150	1,180										
20	138	13.3	92	.2	1,680	2,340	2,640	2,830	2,960	3,060	3,120								
15	103	10	69	.2	3,800	5,650	6,550	7,150	7,500	7,750	7,950	8,080	8,190	8,340	8,420				
30	207	15	103	.33	810	1,050	1,130	1,170											
25	172	12.5	86	.33	1,500	2,060	2,320	2,470	2,570	2,630	2,680								
20	138	10	69	.33	3,040	4,260	4,900	5,280	5,550	5,720	5,850	5,940							
15	103	7.5	52	.33	7,350	10,100	11,700	12,800											
10	69	5	34	.33	16,100	23,700	28,900	32,600	35,500	37,800	39,500	40,800	42,000	43,500	44,500				
30	207	10	69	.5	2,230	3,040	3,430	3,660	3,810	3,920	3,990								
25	172	8.3	57	.5	4,100	5,600	6,380	6,800	7,100	7,260	7,380	7,480	7,500						
20	138	6.7	46	.5	9,500	12,400	13,820	14,730	15,400										
15	103	5	34	.5	18,500	28,000	32,800	35,600	37,600	39,000	40,000	40,800	41,400	42,000	42,500				
10	69	3	21	.5	105,000	140,000	160,000	175,000	185,000	192,500	197,500	202,500	205,000	212,000	215,000	217,500			
30	207	5	34	.7	12,300	16,300	18,300	19,400	20,200	20,700	21,000								
25	172	4.4	30	.7	19,800	27,000	30,900	33,000	34,200	35,200	36,000	36,500							
20	138	3	21	.7	69,000	97,000	112,000	121,000	127,000	130,000	134,000	136,000	138,000	141,000	143,000	144,000			
15	103	3	21	.7	74,000	98,000	115,000	125,000	132,000	137,000	141,000	144,000	147,000	150.000	152,000	153,000	154,000		
10	69	1.7	12	.7	780,000	1,260,000	1,540,000	1,690,000	1,780,000	1,825,000	1,850,000	1,870,000	1,885,000	1,915,000	1,930,000	1,935,000			
30	207	3	21	.8	42,500	58,750	68,750	75,000	77,500	80,000	82,000	83,750	84,000	85,000					
25	172	2.8	19	.8	71,000	94,000	106,000	111,000	116,000	120,000	122,000	123,000	124,000	126,000					

TABLE III.- CRACK AND LOAD MEASUREMENTS AND K_c VALUES FROM RESIDUAL STATIC STRENGTH TESTS ON 7075-T6 ALUMINUM-ALLOY SHEET

a_i		a_f		P_i		P_f		K_c	
in.	mm	in.	mm	kips	kN	kips	kN	ksi-$in^{1/2}$	$MN/m^{3/2}$
1.72	43.67	1.85	46.99	23.4	104	29.9	133	39.2	43.1
1.59	40.39	1.80	45.72	17.7	79	30.4	135	39.2	43.1
1.53	38.86	1.79	45.34	20.0	89	30.4	135	38.5	42.3
1.94	49.15	2.36	59.95	16.5	73	27.2	121	39.8	43.7
1.02	25.91	1.16	29.47	----	---	38.5	171	38.0	41.7
.98	24.89	1.19	30.10	----	---	38.8	173	39.7	43.7
.91	22.99	.96	24.39	----	---	43.1	192	38.0	41.7
1.01	25.65	1.09	27.56	----	---	41.7	185	41.4	45.5
1.05	26.67	1.15	29.21	29.2	130	37.7	168	38.4	42.2
.78	19.81	.94	23.75	32.8	146	44.5	198	41.6	45.7
1.31	33.27	1.75	44.45	19.2	85	32.0	142	40.2	44.2
1.90	48.26	2.19	55.63	15.7	70	25.0	111	35.4	39.0
.52	13.21	.73	18.42	32.8	146	50.4	224	40.4	44.4
1.22	30.99	1.53	38.86	25.8	115	35.9	160	42.0	46.2
1.76	44.71	2.10	53.34	18.3	81	30.2	134	41.8	45.9
1.40	35.44	1.73	43.82	26.8	119	32.3	144	41.0	45.1
1.17	29.59	1.43	36.20	29.2	130	36.4	162	40.2	44.2
.54	13.72	.71	17.91	33.3	148	49.8	222	38.5	42.3
1.51	38.23	1.65	41.91	24.0	107	39.0	173	47.6	52.3
2.25	57.15	2.73	69.34	12.3	54	24.3	108	41.0	45.0
2.47	62.87	2.81	71.38	14.0	62	22.8	101	39.0	42.9
1.78	45.09	2.13	53.98	14.8	66	27.1	121	39.0	42.9
.70	17.78	.93	23.50	----	---	47.1	210	43.4	47.7
.53	13.46	.78	19.69	29.4	131	48.4	215	40.3	44.3
1.07	27.18	1.20	30.48	30.0	133	39.0	173	48.2	52.9
1.12	28.32	1.37	34.80	30.0	133	36.0	160	39.4	43.3
.55	13.97	.72	18.29	----	---	47.5	211	37.6	41.3

TABLE IV.- TRANSITION CRACK LENGTHS AND CRACK-GROWTH RATES FOR R VALUES FROM -1.0 TO 0.8 FOR 7075-T6 ALUMINUM-ALLOY SHEET

S'_m		S'_a		Nominal R value	a_t		da/dN at transition		ΔK_t		Type of shear
ksi	MN/m^2	ksi	MN/m^2		in.	mm	in./cycle	nm/cycle	ksi-$in^{1/2}$	$MN/m^{3/2}$	
0	0	30	207	-1	≤0.05	≤1.3	----------	---	---	---	Dual
0	0	30	207	-1	≤.05	≤1.3	----------	---	---	---	Single
0	0	25	172	-1	≤.05	≤1.3	----------	---	---	---	Dual
0	0	25	172	-1	≤.05	≤1.3	----------	---	---	---	Single
0	0	20	138	-1	≤.05	≤1.3	----------	---	---	---	Dual
0	0	20	138	-1	-----	----	----------	---	---	---	------
0	0	15	103	-1	.13	3.3	1.08×10^{-5}	274	5.4	5.9	Dual
0	0	15	103	-1	.17	4.3	1.49×10^{-5}	379	6.3	6.9	Single
0	0	10	69	-1	.37	9.4	1.37×10^{-5}	348	6.0	6.6	Double
0	0	10	69	-1	-----	----	----------	---	---	---	------
0	0	5	34	-1	1.16	58.9	9.67×10^{-6}	246	5.4	5.9	Double
0	0	5	34	-1	1.64	41.7	1.64×10^{-5}	417	6.5	7.1	Dual
2.5	17	20	138	-.8	≤.05	≤1.3	----------	---	---	---	Dual
2.5	17	20	138	-.8	≤.05	≤1.3	----------	---	---	---	Single
2.5	17	17.5	121	-.8	≤.05	≤1.3	----------	---	---	---	Dual
2.5	17	17.5	121	-.8	.12	3.1	1.18×10^{-5}	300	6.9	7.6	Dual
5	34	25	172	-.7	≤.05	≤1.3	----------	---	---	---	Single
5	34	25	172	-.7	≤.05	≤1.3	----------	---	---	---	Double
2.5	17	15	103	-.7	.18	4.6	2.53×10^{-5}	643	7.3	8.0	Dual
2.5	17	15	103	-.7	.20	5.1	2.78×10^{-5}	706	7.8	8.6	Dual
2.5	17	12.5	86	-.7	.16	4.1	1.03×10^{-5}	262	5.9	6.5	Dual
2.5	17	12.5	86	-.7	.28	7.1	2.31×10^{-5}	587	7.9	8.7	Dual
5	34	20	138	-.6	≤.05	≤1.3	----------	---	---	---	Double
5	34	20	138	-.6	.10	2.5	2.31×10^{-5}	587	7.9	8.7	Dual
2.5	17	10	69	-.6	.22	5.6	1.24×10^{-5}	315	5.8	6.4	Dual
2.5	17	10	69	-.6	.31	7.9	2.09×10^{-5}	531	6.9	7.6	Double
5	34	15	103	-.5	≤.05	≤1.3	----------	---	---	---	Single
5	34	15	103	-.5	≤.05	≤1.3	----------	---	---	---	Single
10	69	20	138	-.33	≤.05	≤1.3	----------	---	---	---	Single
10	69	20	138	-.33	≤.05	≤1.3	----------	---	---	---	Dual
5	34	10	69	-.33	.17	4.2	9.48×10^{-6}	241	6.1	6.7	Single
5	34	10	69	-.33	.21	5.3	1.27×10^{-5}	323	6.8	7.5	Single
2.5	17	5	34	-.33	.67	17.0	1.49×10^{-5}	379	6.0	6.6	Double
2.5	17	5	34	-.33	.77	14.6	1.54×10^{-5}	391	6.5	7.1	Double
20	138	30	207	-.2	≤.05	≤1.3	----------	---	---	---	Dual
20	138	30	207	-.2	≤.05	≤1.3	----------	---	---	---	Dual
10	69	15	103	-.2	≤.05	≤1.3	----------	---	---	---	Single
10	69	15	103	-.2	≤.05	≤1.3	----------	---	---	---	Dual
15	103	20	138	-.14	≤.05	≤1.3	----------	---	---	---	Single
15	103	20	138	-.14	≤.05	≤1.3	----------	---	---	---	Dual

TABLE IV.- TRANSITION CRACK LENGTHS AND CRACK-GROWTH RATES FOR R VALUES

FROM -1.0 TO 0.8 FOR 7075-T6 ALUMINUM-ALLOY SHEET - Concluded

S'_m		S'_a		Nominal R value	a_t		da/dN at transition		ΔK_t		Type of shear
ksi	MN/m^2	ksi	MN/m^2		in.	mm	in./cycle	nm/cycle	$ksi\text{-}in^{1/2}$	$MN/m^{3/2}$	
25	172	25	172	0	≤ 0.05	≤ 1.3	----------	---	---	---	Dual
25	172	25	172	0	$\leq .05$	≤ 1.3	----------	---	---	---	Double
20	138	20	138	0	$\leq .05$	≤ 1.3	----------	---	---	---	Dual
20	138	20	138	0	$\leq .05$	≤ 1.3	----------	---	---	---	Dual
15	103	15	103	0	$\leq .05$	≤ 1.3	----------	---	---	---	Dual
15	103	15	103	0	$\leq .05$	≤ 1.3	----------	---	---	---	Dual
10	69	10	69	0	.11	2.8	1.06×10^{-5}	269	6.5	7.1	Double
10	69	10	69	0	.13	3.3	1.44×10^{-5}	379	7.1	7.8	Single
5	34	5	34	0	.52	13.2	1.53×10^{-5}	389	7.1	7.8	Dual
5	34	5	34	0	.61	15.5	2.54×10^{-5}	645	7.7	8.5	Dual
30	207	20	138	.2	$\leq .05$	≤ 1.3	----------	---	---	---	Single
30	207	20	138	.2	$\leq .05$	≤ 1.3	----------	---	---	---	Single
25	172	16.7	115	.2	$\leq .05$	≤ 1.3	----------	---	---	---	Single
25	172	16.7	115	.2	$\leq .05$	≤ 1.3	----------	---	---	---	Double
20	138	13.3	92	.2	$\leq .05$	≤ 1.3	----------	---	---	---	Dual
20	138	13.3	92	.2	$\leq .05$	≤ 1.3	----------	---	---	---	Dual
15	103	10	69	.2	.08	2.0	Crack length too short to measure rate				Single
15	103	10	69	.2	.11	2.8	1.96×10^{-5}	498	6.5	7.1	Single
30	207	15	103	.33	$\leq .05$	≤ 1.3	----------	---	---	---	Single
30	207	15	103	.33	$\leq .05$	≤ 1.3	----------	---	---	---	Double
25	172	12.5	86	.33	$\leq .05$	≤ 1.3	----------	---	---	---	Dual
25	172	12.5	86	.33	$\leq .05$	≤ 1.3	----------	---	---	---	Dual
20	138	10	69	.33	$\leq .05$	≤ 1.3	----------	---	---	---	Dual
20	138	10	69	.33	.10	2.7	2.31×10^{-5}	587	6.3	6.9	Double
15	103	7.5	52	.33	.15	3.8	1.90×10^{-5}	483	5.8	6.4	Dual
15	103	7.5	52	.33	.15	3.8	1.33×10^{-5}	338	5.8	6.4	Double
10	69	5	34	.33	.31	7.9	1.72×10^{-5}	437	5.6	6.2	Single
10	69	5	34	.33	.32	8.1	1.88×10^{-5}	478	5.7	6.3	Double
30	207	10	69	.5	$\leq .05$	≤ 1.3	----------	---	---	---	Dual
30	207	10	69	.5	$\leq .05$	≤ 1.3	----------	---	---	---	Single
25	172	8.3	57	.5	$\leq .05$	≤ 1.3	----------	---	---	---	Dual
25	172	8.3	57	.5	$\leq .05$	≤ 1.3	----------	---	---	---	Double
20	138	6.7	46	.5	.18	4.6	1.80×10^{-5}	457	5.5	6.0	Double
20	138	6.7	46	.5	.21	5.3	2.10×10^{-5}	533	6.1	6.7	Double
15	103	5	34	.5	.21	5.3	8.08×10^{-6}	205	4.6	5.1	Dual
15	103	5	34	.5	.30	7.6	2.00×10^{-5}	508	5.5	6.0	Double
10	69	3	21	.5	.56	14.2	1.14×10^{-5}	290	4.5	4.9	Dual
10	69	3	21	.5	.84	21.2	1.86×10^{-5}	472	5.5	6.0	Single
30	207	5	34	.7	.17	4.3	1.07×10^{-5}	273	4.1	4.5	Double
30	207	5	34	.7	.25	6.4	2.54×10^{-5}	622	5.0	5.5	Single
25	172	4.4	30	.7	----	----	----------	---	---	---	------
25	172	4.4	30	.7	.27	6.9	1.69×10^{-5}	429	4.5	4.9	Double
20	138	3	21	.7	.44	11.1	1.21×10^{-5}	307	3.9	4.3	Dual
20	138	3	21	.7	.50	12.7	1.72×10^{-5}	437	4.2	4.6	Dual
15	103	3	21	.7	----	----	----------	---	---	---	------
15	103	3	21	.7	.57	14.5	1.58×10^{-5}	401	4.6	5.1	Dual
10	69	1.7	12	.7	1.44	36.6	2.88×10^{-5}	731	4.1	4.5	Double
10	69	1.7	12	.7	1.53	38.9	2.55×10^{-5}	648	4.3	4.7	Double
30	207	3	21	.8	----	----	----------	---	---	---	------
30	207	3	21	.8	.43	10.9	1.92×10^{-5}	488	4.0	4.4	Double
25	172	2.8	19	.8	.42	10.7	1.35×10^{-5}	343	3.6	4.0	Double
25	172	2.8	19	.8	.55	13.9	2.20×10^{-5}	559	4.1	4.5	Dual

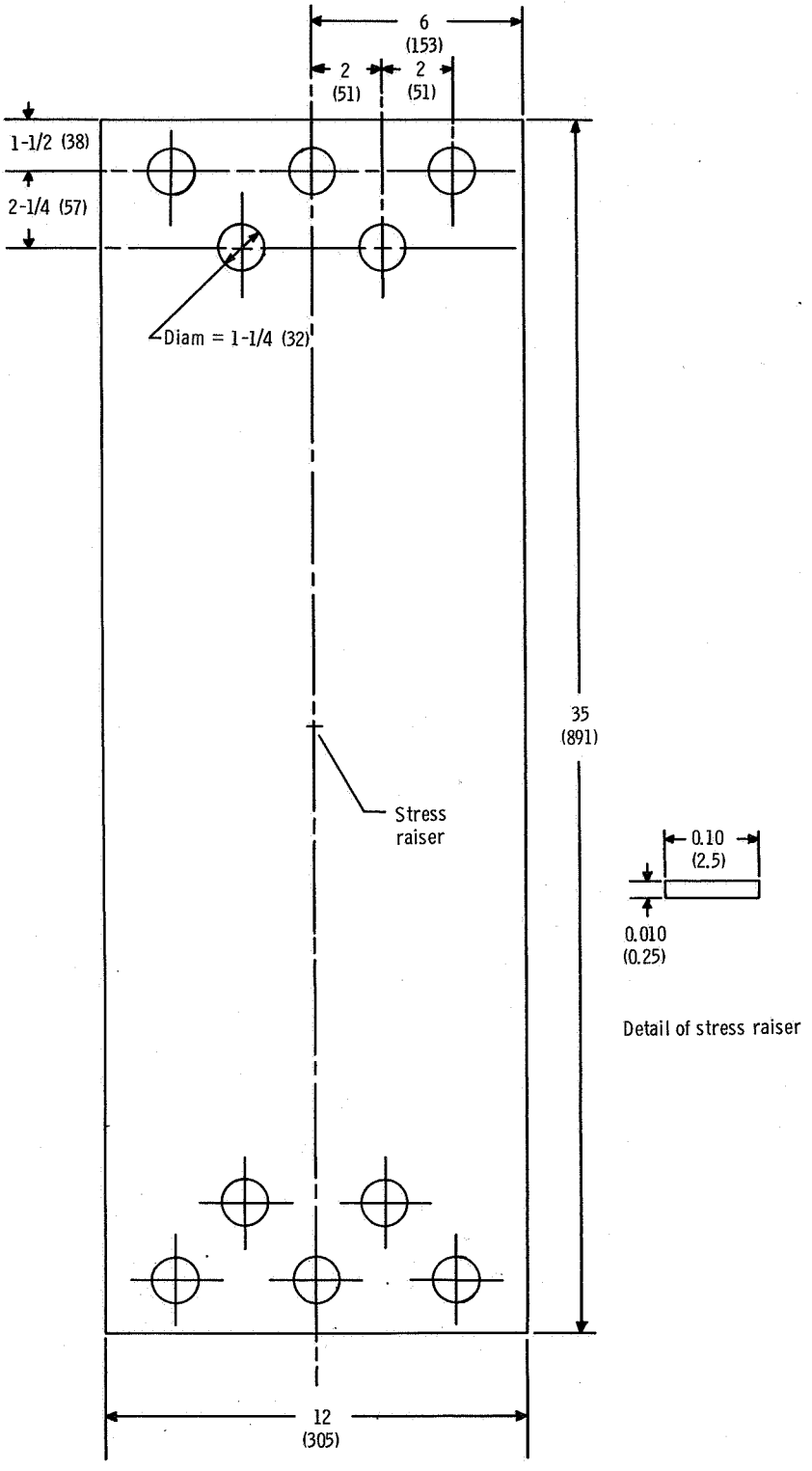

Figure 1.- Specimen configuration. All dimensions are in inches (mm).

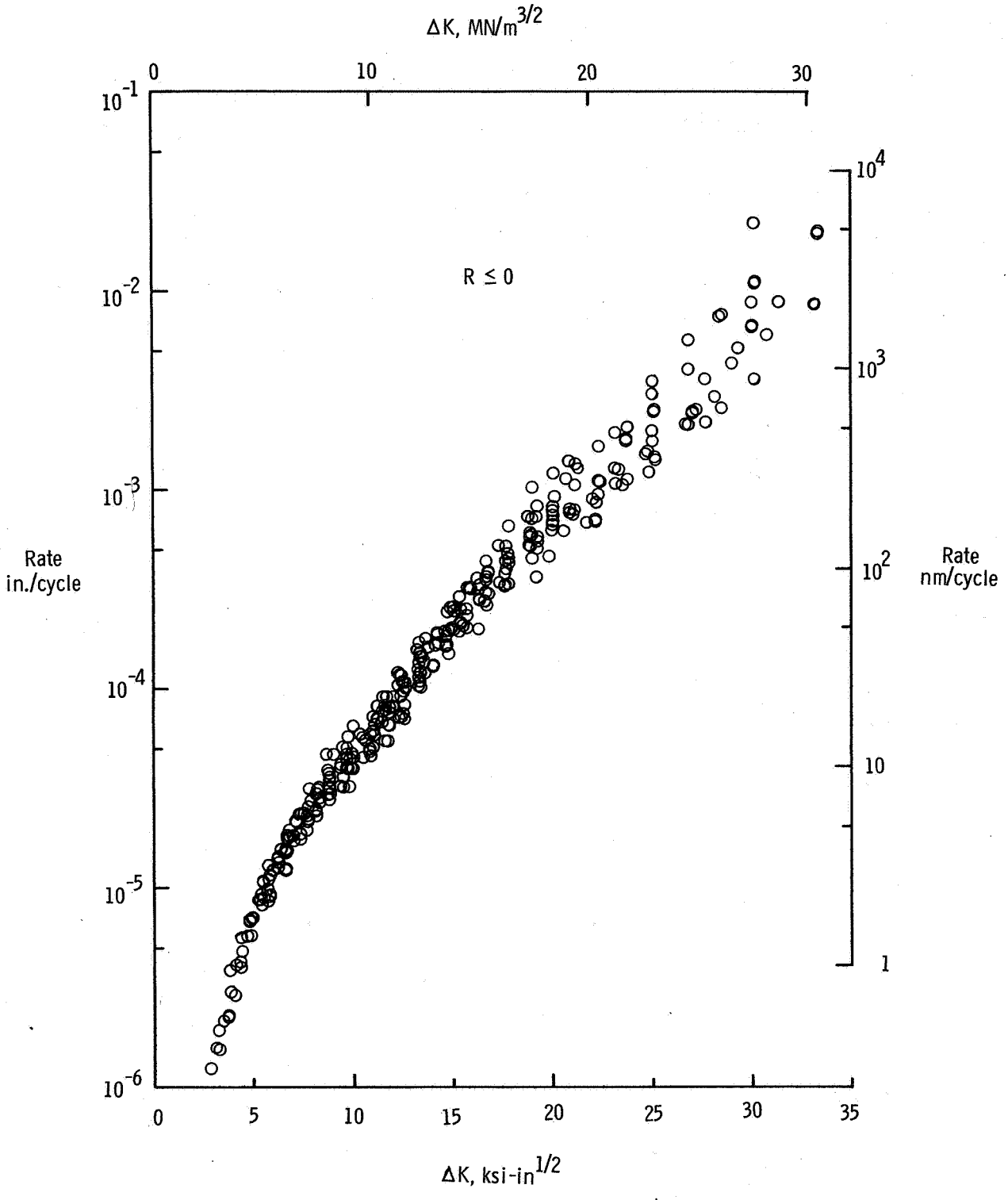

Figure 2.- Variation of fatigue crack growth rate with ΔK for $R \leq 0$.

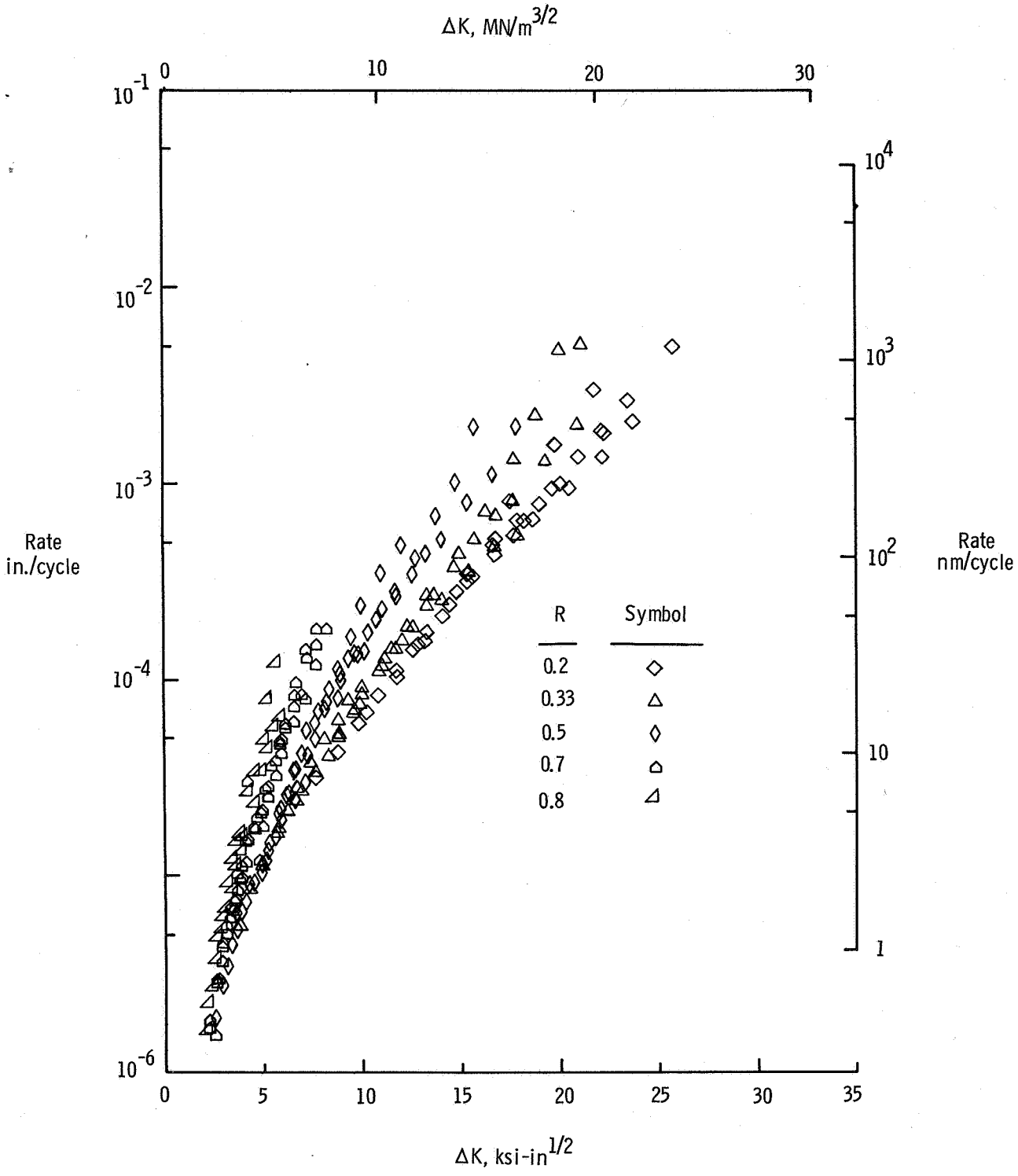

Figure 3.- Variation of fatigue crack growth rate with ΔK for $R > 0$.

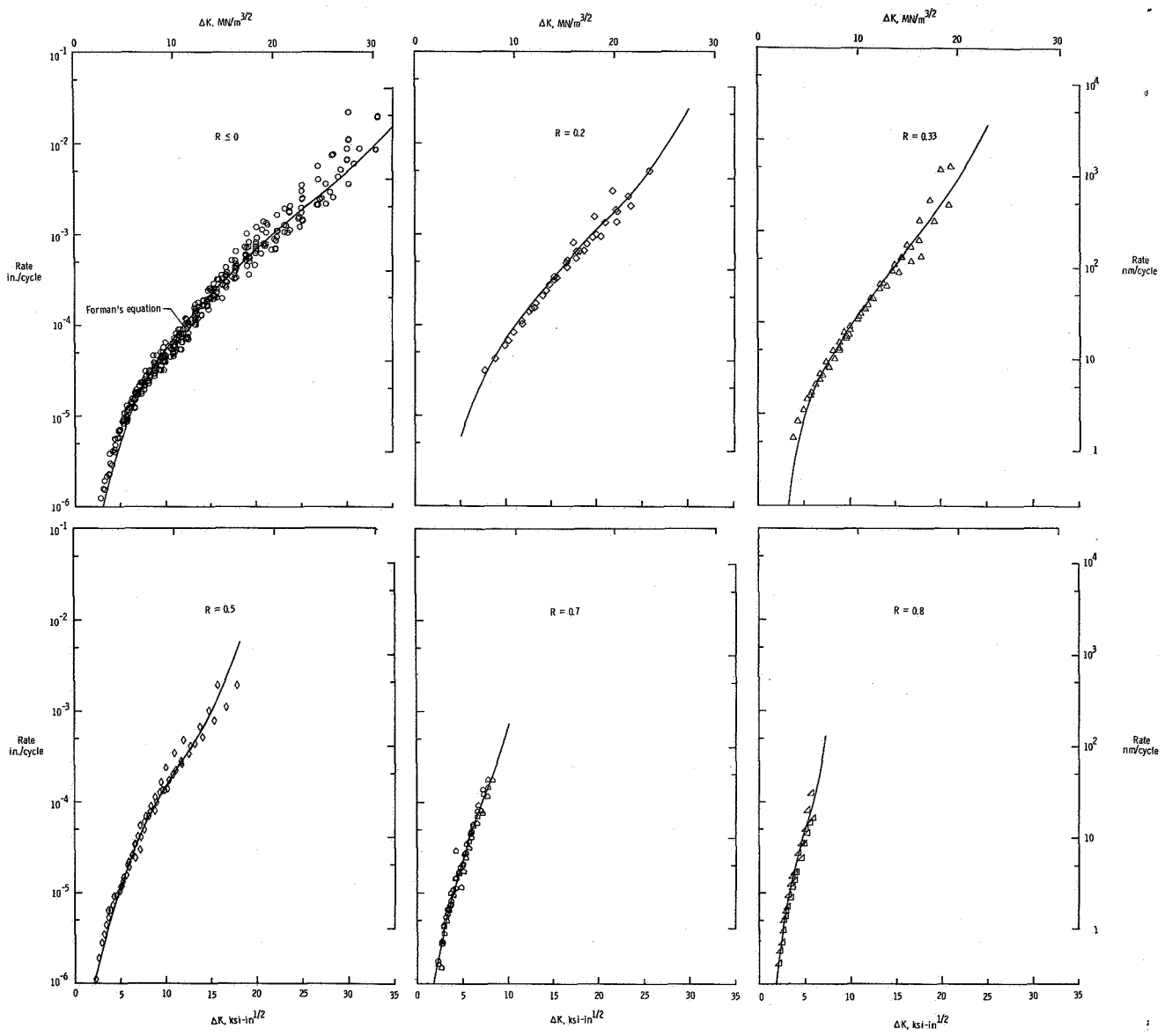

Figure 4.- Correlation of experimental fatigue crack growth rates at various stress ratios with Forman's equation.

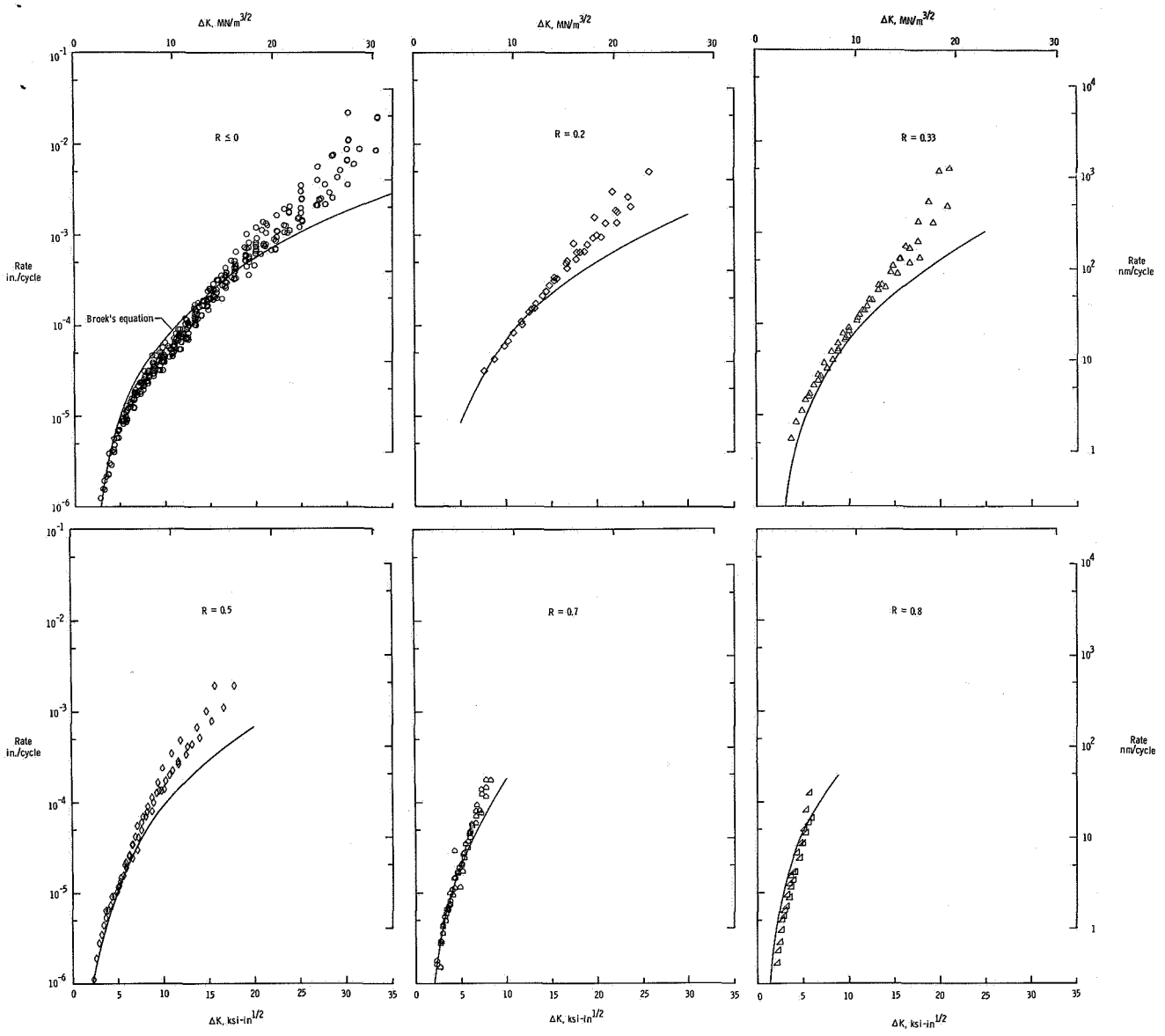

Figure 5.- Correlation of experimental fatigue crack growth rates at various stress ratios with Broek and Schijve's equation.

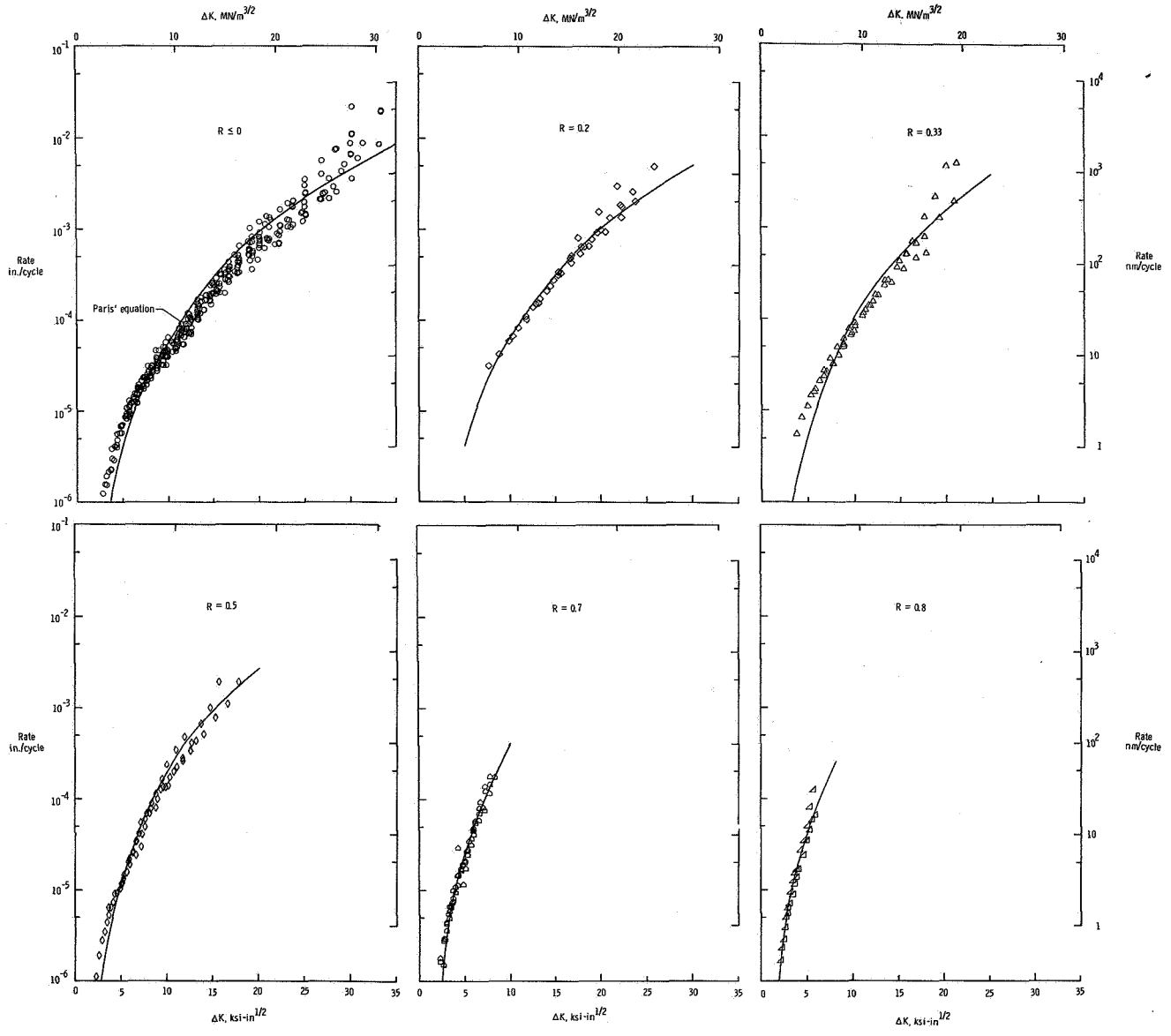

Figure 6.- Correlation of experimental fatigue crack growth rates at various stress ratios with Paris' equation.

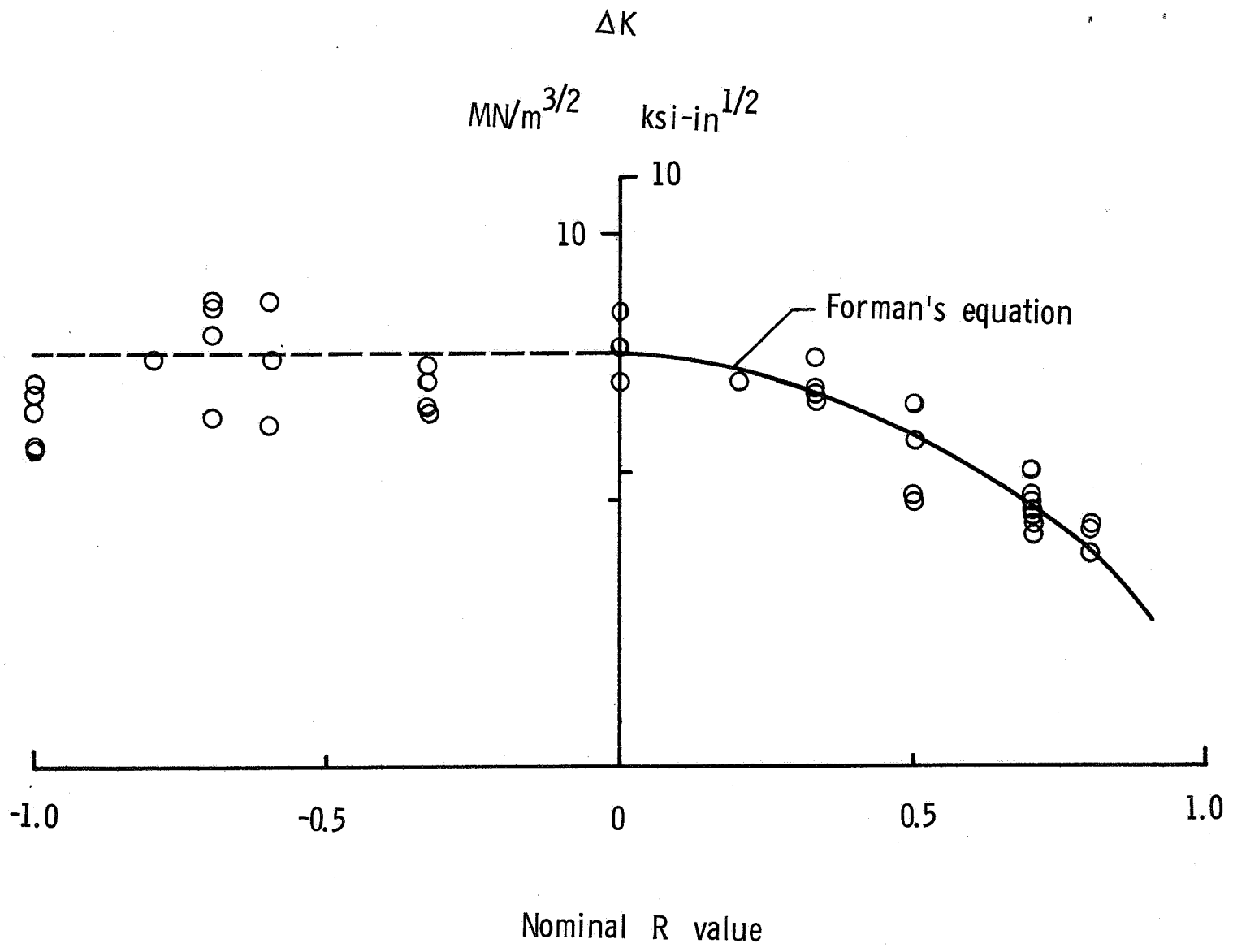

Figure 7.- Variation of the stress intensity range at transition from the normal mode to the shear mode with stress ratio.